The effect of non-magnetic dilution of the Tb sublattice in $TbCo_3B_2$

2010 J. Phys.: Condens. Matter 22 026001

(http://iopscience.iop.org/0953-8984/22/2/026001)

J. Phys.: Condens. Matter **22** (2010) 026001 (7pp) doi:10.1088/0953-8984/22/2/026001

The effect of non-magnetic dilution of the Tb sublattice in $TbCo_3B_2$

Erez J Wolfson[1,5], El'ad N Caspi[2], Hanania Ettedgui[2], Hagai Shaked[3] and Maxim Avdeev[4]

[1] Department of Nuclear Engineering, Ben-Gurion University of the Negev, PO Box 653, Beer-Sheva 84105, Israel
[2] Nuclear Research Centre—Negev, PO Box 9001, Beer-Sheva 84190, Israel
[3] Department of Physics, Ben-Gurion University, PO Box 653, Beer-Sheva 84105, Israel
[4] Bragg Institute, ANSTO, PMB 1, Menai, NSW 2234, Australia

E-mail: ejwolf@gmail.com and wolfsoy@bgu.ac.il

Received 27 August 2009, in final form 26 October 2009
Published 9 December 2009
Online at stacks.iop.org/JPhysCM/22/026001

Abstract

Solid solutions of $Tb_{1-x}Y_xCo_3B_2$ ($x = 0.05$, 0.1, 0.25, 0.4 and 0.5) were studied by neutron powder diffraction, x-ray diffraction, AC susceptibility and SQUID magnetization measurements. Their magnetic and crystallographic properties were deduced and examined together with those previously published for the end compounds ($x = 0$, 1). These solid solutions have hexagonal symmetry and are paramagnetic at RT, and undergo a magnetic ordering transition of the Co sublattice, with the magnetic moments along the hexagonal axis, at $T_{Co} \sim 150(15)$ K, independent of Y concentration. A second magnetic ordering transition of the Tb sublattice $T_{Tb} \leqslant 30$ K accompanied by the rotation of the magnetic moments towards the basal plane, was observed for solid solutions with Y concentration $x \leqslant 0.25$. This transition was also found to be accompanied by a crystallographic symmetry decrease. Unexpectedly, neutron powder diffraction showed that the magnitude of the ordered magnetic moment of the Tb ion decreases with Tb concentration.

(Some figures in this article are in colour only in the electronic version)

1. Introduction

The compound $TbCo_3B_2$ belongs to the $R_{n+1}Co_{3n+5}B_{2n}$ (R = lanthanide, $n = 0, 1, 2, 3, \infty$) family with $n = \infty$ [1]. At room temperature (RT) it crystallizes in a hexagonal structure with $P6/mmm$ symmetry [2]. In $TbCo_3B_2$ ($CeCo_3B_2$-type structure) the atoms are placed in the following sites (table 1): Tb at 1a, Co at 3g and B at 2c [2]. This compound, paramagnetic at RT, undergoes a high temperature ferromagnetic ordering transition of the Co sublattice at $T_{Co} = 170(15)$ K, with magnetic moments aligned along the c axis. The Tb sublattice orders at a lower temperature, $T_{Tb} = 30(3)$ K, where a spin reorientation transition (SRT) occurs. As temperature is lowered below T_{Tb} the moments rotate towards the basal ab plane [3]. T_{Co} was attributed to the Co–Co exchange interaction while T_{Tb} was attributed to the Tb–Tb exchange interaction. Below T_{Tb}, components of the magnetic moment appear in the ab plane, leading to an orthorhombic distortion of the crystal lattice. Attributing the high temperature transition to the Co–Co exchange interaction was supported by the study of YCo_3B_2 [4], where only the T_{Co} transition was observed. It was also supported by the study of $HoCo_3B_2$ [5], where a ferromagnetic ordering was observed at $T_{Co} \sim 150$ K and ordering accompanied by a spin reorientation was observed at $T_{Ho} \approx 12$ K. The latter is attributed to an Ho–Ho exchange interaction similar to a Tb–Tb exchange interaction for $TbCo_3B_2$. In order to study the T_{Tb} dependence on the magnetic properties of the R atom and to decouple the Co–Co (T_{Co}) from the Tb–Tb (T_{Tb}) transitions, five samples of $Tb_{1-x}Y_xCo_3B_2$ ($x = 0.05$, 0.1, 0.25, 0.4 and 0.5) were prepared and studied by various magnetic and crystallographic methods. The results were compared with the published results of the end compounds (i.e. $x = 0$ and 1).

[5] Author to whom any correspondence should be addressed.

Table 1. Unit cell basis of the $P6/mmm$, $Cmmm$ and $C2/m$ phases and their atomic sites. The unit cells are defined with respect to the fundamental lattice vector of $P6/mmm$.

Space group		$P6/mmm(191)$		$Cmmm(65)$		$C2/m(12)$	
Unit cell basis	a	(1, 0, 0)		(2, 1, 0)		(2, 1, 0)	
	b	(0, 1, 0)		(0, 1, 0)		(0, $\bar{1}$, 0)	
	c	(0, 0, 1)		(0, 0, 1)		(0, 0, $\bar{1}$)	
Coordinates	Tb/Y	1a	0, 0, 0	2a	0, 0, 0	2a	0, 0, 0
	Co	3g	$\frac{1}{2}$, 0, $\frac{1}{2}$	2c	$\frac{1}{2}$, 0, $\frac{1}{2}$	2d	0, $\frac{1}{2}$, $\frac{1}{2}$
				4f	$\frac{1}{4}$, $\frac{1}{4}$, $\frac{1}{2}$	4f	$\frac{1}{4}$, $\frac{1}{4}$, $\frac{1}{2}$
	B	2c	$\frac{1}{3}$, $\frac{2}{3}$, 0	4g	x, 0, 0 ($x \approx \frac{1}{3}$)	4i	x, 0, z ($x \approx \frac{1}{3}$; $z \approx 0$)

2. Experimental details

Samples of $Tb_{1-x}Y_xCo_3B_2$ ($x = 0.05$, 0.1, 0.25, 0.4 and 0.5) were prepared by arc melting the constituents in an argon atmosphere followed by a subsequent annealing at 1200–1300 K in vacuum for ∼120 h. ^{11}B was used to minimize absorption of thermal neutrons. The sample was characterized by x-ray diffraction (XRD).

Measurements of AC magnetic susceptibility were carried out from RT down to 5 K on the five samples ($x = 0.05$, 0.1, 0.25, 0.4 and 0.5) and compared with previously measured (using the same instrument) end compounds ($x = 0$ and 1) [3, 4]. The amplitude of the applied AC ($f \sim 1.5$ kHz) magnetic field was 10 Oe. Calibration of the AC susceptometer was done in the temperature range 7 K $< T <$ 300 K using a 42 mg powder sample of Ho_2O_3 (RT molar susceptibility $\chi_M \sim 89 \times 10^{-3}$ emu mol^{-1}). Liquid He was used for cooling. In addition, SQUID magnetization measurements were performed at 4–300 K and with $H = 10$ kOe, using the Quantum Design MPMS5 instrument in the Racah Institute of Physics at the Hebrew University of Jerusalem.

Neutron powder diffraction (NPD) measurements were carried out using the medium resolution neutron powder diffractometer (MRPD) and the high resolution neutron powder diffractometer (HRPD) at the high flux Australian reactor operated by the Australian Nuclear Science and Technology Organization. The MRPD ($\lambda = 1.665(1)$ Å, $2\theta = 2°$–$138°$, step 0.1°) data was preferred for the magnetic study due to the higher neutron flux, while the HRPD ($\lambda = 1.492(1)$ Å, $2\theta = 10°$–$150°$, step 0.05°) data was used, due to its higher resolution, to study the crystallographic properties in detail. Four samples ($x = 0.05$, 0.1, 0.25 and 0.5) were measured using the MRPD at RT before cooling down to the lowest temperature (LT) in the range of 6.5–7 K. NPD data were collected upon heating at about 20 temperatures for each sample. Due to the limited resolution of the MRPD, two of those sample ($x = 0.1$ and 0.25) were also measured using the HRPD, for higher accuracy of crystallographic parameter determination. No NPD measurement was carried out for $x = 0.4$. Both XRD and NPD data were analyzed using the Rietveld refinement method with the FULLPROF code [6, 7].

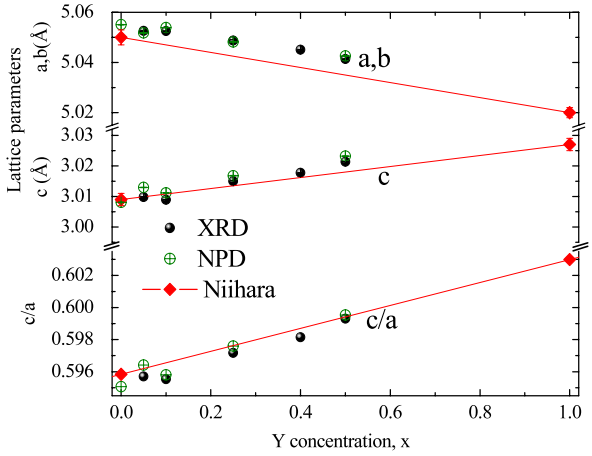

Figure 1. Lattice parameters (a, b), (c) and c/a of $Tb_{1-x}Y_xCo_3B_2$ determined by Rietveld refinement of XRD (closed circles), NPD (open circles) and Niihara's [8] (diamonds). The lines represent the prediction by Vegard's law deduced from Niihara. The error bars are smaller than the symbol's size.

3. Results and analysis

The observed reflections in the RT x-ray diffraction patterns of four samples ($x = 0.05$, 0.25, 0.4 and 0.5) proved the high quality of the compounds. The impurities were found to be negligible and the crystallographic parameters (a, c) were found to be in excellent agreement with Vegard's law, deduced from the end compound results according to Niihara [8] (figure 1). This result supports our hypothesis that the Y is properly incorporated into the compounds. In the diffraction pattern of the $x = 0.1$ sample small unidentified impurity lines were found (<1% of strongest line). The existence of this impurity in the $x = 0.1$ sample may indicate imperfections in the crystallization of the main phase (e.g. vacancies), and therefore may be the origin of the slight disagreement of this sample's refined cell parameters with Vegard's law (figure 1).

In the measurements of the molar AC susceptibility, χ_M, versus temperature, an anomaly at $T_{Co} \approx 150$ K was observed in all samples except for $x = 0.1$ (figure 2). The distinctive behavior of this sample might be related to the existence of an impurity phase in the sample (as was mentioned above).

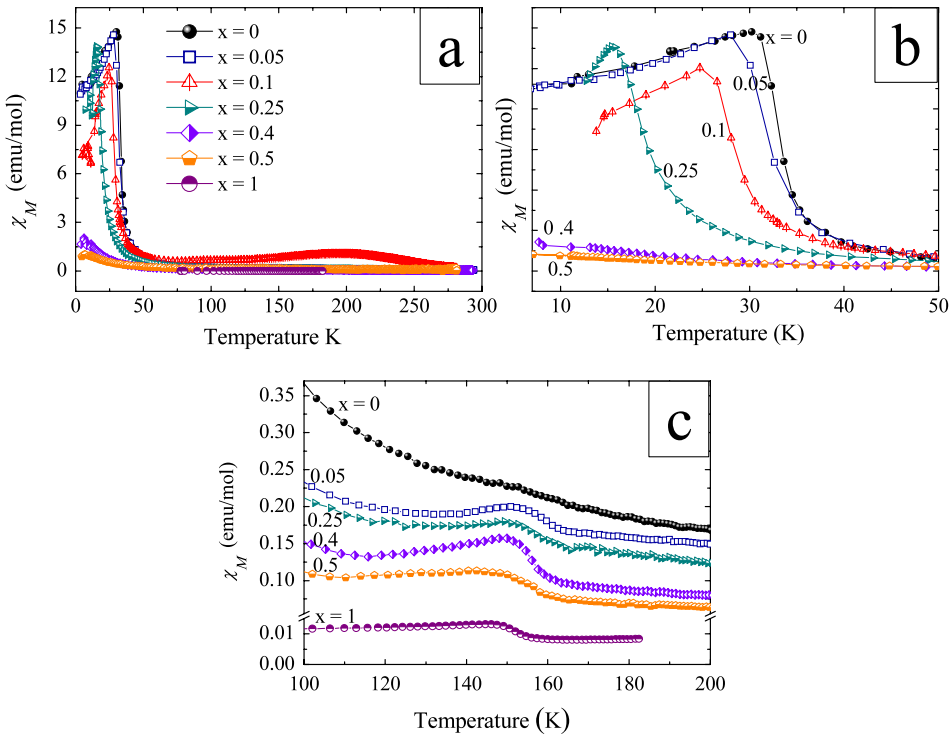

Figure 2. (a) Molar AC susceptibilities, χ_M, of the five samples along with the two end compounds as a function of temperature. (b) Zoom-in of the T_{Tb} region. (c) Zoom-in of the 100–200 K region. The data for the end compounds ($x = 0$ and 1) were taken from previous studies [3, 4]. The result of the $x = 0.1$ sample is not shown in (c), due to its signal being beyond the scale.

The anomaly in the range of $T_{Co} \approx 150$ K was also observed in both end compounds $TbCo_3B_2$ [3] and YCo_3B_2 [4], where it was attributed to the paramagnetic–ferromagnetic transition in the Co sublattice. Thus, the present AC susceptibility measurements support our previous suggestion [3, 5] that the ferromagnetic ordering of the Co at T_{Co} is independent of Y concentration. This is unlike T_{Tb}, which decreases almost linearly with the increase of Y concentration until it vanishes in the vicinity of $x = 0.4$ (figures 2 and 3). This decrease is anticipated as a result of the dilution of the Tb sublattice by the non-magnetic Y atoms (see section 4). SQUID magnetization measurements of the same samples (not shown) are in good agreement with the AC results (figure 3).

The NPD data collected above T_{Tb} were analyzed using the $P6/mmm$ space group (table 1). The analysis of the NPD data collected at MRPD for $x = 0.05$, 0.1, 0.25 and 0.5 samples at RT (table 2) yielded lattice parameters in good agreement with XRD-refined values (figure 1). When cooled down to LT, a significant intensity increase in some of the NPD reflections was observed for $x = 0.05$, 0.1 and 0.25 samples (e.g. {100} and {101} (figure 4)). This increase in intensity is presumably related to the magnetic ordering transition observed in the magnetic measurements (cf figure 2). The integral intensity of the line with the highest intensity increase ({100} figure 4) is presented in figure 5 as a function of temperature. The observed transition temperatures (figure 5) decrease as x increases, and are in good agreement with the T_{Tb} as observed in the magnetic measurements (figure 3).

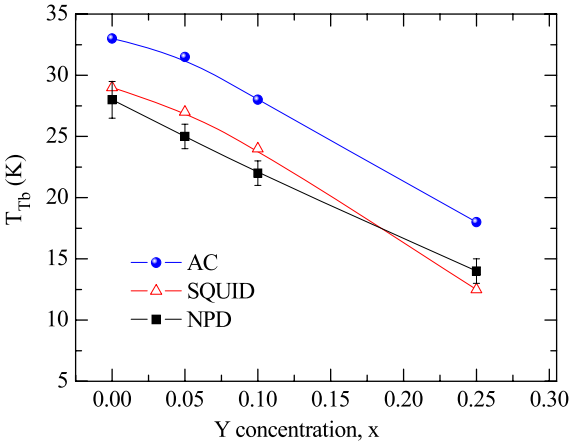

Figure 3. T_{Tb} as a function of Y concentration measured by AC, SQUID and NPD. The constant difference between T_{Tb} measured by the SQUID and NPD and the T_{Tb} measured by the AC is due to the nature of each measurement. While SQUID and NPD measure the magnetization the AC measures the susceptibility directly (dM/dH). The error bars of AC and SQUID are smaller than the symbol's size.

4. LT NPD analysis

In refining the crystallographic and magnetic parameters to fit the diffraction patterns observed below T_{Tb}, a collinear magnetic model was considered. In this model, the Tb and Co sublattices are each ferromagnetic. The magnetic axes of the two sublattices are allowed to be either parallel (ferromagnetic) or antiparallel (ferrimagnetic) to each other

Table 2. Refined values of structural and magnetic parameters of the four samples from the MRPD, at RT (a) and LT (b) temperatures. Previously collected [9] data also used for the refinement of the $x = 0.25$ sample. (a) The a and c are lattice parameters (atomic positions are presented in table 1). $B_{Tb/Y}$, B_{Co} and B_B are the isotropic thermal factors. χ^2, R_p and R_{wp} are the reliability factor, weighted profile factor and weighted squared difference [7]. Numbers in parentheses are standard deviations of the last significant digit. (b) The a, b and c are lattice parameters, x (B) and z (B) are the boron coordinates and β is the angle between c axis and ab plane. μ_{Tb}, μ_{Co} and θ are, respectively, the Tb and Co magnetic moments and their angle to the hexagonal axis.

Sample, x		0.05	0.1	0.25	0.5
(a) RT results					
Space group		$P6/mmm$	$P6/mmm$	$P6/mmm$	$P6/mmm$
Temperature	(K)	300	300	300	300
a	(Å)	5.05049(9)	5.0563(1)	5.04641(8)	5.04148(7)
c	(Å)	3.01193(7)	3.0127(1)	3.01640(7)	3.02281(6)
$B_{Tb/Y}$	(Å^2)	0.7(1)	0.7(1)	0.68(7)	0.536(7)
B_{Co}	(Å^2)	0.48(8)	0.70(12)	0.61(7)	0.41(7)
B_B	(Å^2)	0.82(5)	0.66(9)	0.91(5)	0.87(5)
Reliability factors:					
χ^2		0.838	0.497	0.801	0.721
R_p		3.23	4.41	3.47	3.68
R_{wp}		4.24	5.63	4.63	4.72
(b) LT results					
Crystallographic parameters:					
Space group		$C2/m$	$C2/m$	$C2/m$	$P6/mmm$
Temperature	(K)	6.5	6.5	7	5.5
a	(Å)	8.7345(6)	8.7480(6)	8.7334(2)	5.03761(7)
b	(Å)	5.0484(3)	5.0496(3)	5.04138(9)	—
c	(Å)	3.00213(5)	3.00107(8)	3.00616(4)	3.01342(6)
β	(deg)	90.116(4)	90.099(1)	90.0300(7)	—
x (B)		0.331(2)	0.333(1)	0.3336(3)	—
z (B)		0.005(5)	0.0149(4)	0.000(4)	—
$B_{Tb/Y}$	(Å^2)	0.47(6)	0.6(1)	0.51(6)	0.43(7)
B_{Co}	(Å^2)	0.40(5)	0.60(9)	0.77(5)	0.46(7)
B_B	(Å^2)	0.71(5)	0.42(7)	0.75(4)	0.67(5)
Magnetic parameters:					
Space group		$P1$	$P1$	$P1$	—
μ_{Tb}	(μ_B)	5.07(5)	4.13(9)	2.4(1)	—
μ_{Co}	(μ_B)	−0.010(7)	−0.03(3)	−0.10(6)	—
θ	(deg)	76(2)	46(3)	50(6)	—
Reliability factors:					
χ^2		0.950	0.677	0.697	1.31
R_p		2.69	3.97	2.79	3.5
R_{wp}		3.42	5.19	3.56	4.72

and are aligned with an angle θ to the hexagonal axis. This model was previously found in $TbCo_3B_2$ to be in the ferrimagnetic state [3]. The basal plane component of the magnetic moment does not conform with hexagonal symmetry. Therefore, SRT (where $\theta \neq 0$) must be accompanied by a symmetry decrease as was found in $TbCo_3B_2$ [3], where an orthorhombic distortion was observed and an orthorhombic $Cmmm$ unit cell was used to describe the crystallographic structure below T_{Tb} [10]. Furthermore, with $0° < \theta < 90°$, the magnetic symmetry is lower than orthorhombic. Thus, a further symmetry decrease must be taken into consideration for the structure found below T_{Tb}. The maximal subgroup of $Cmmm$ consistent with $0° < \theta < 90°$ is the monoclinic $C2/m$ space group, with the formal magnetic space group $C2'/m'$ [10].

Hence, three models, in which the crystallographic structure is either $P6/mmm$, $Cmmm$ or $C2/m$ (henceforth *hexagonal*, *orthorhombic* or *monoclinic*, respectively), were refined in order to find which crystallographic space group best fits the NPD patterns of each sample. The magnetic structure in the three models were described by magnetic phases containing only magnetic atoms using the $P1$ space group. Refinements of the $x = 0.05$ sample data measured at MRPD yielded significantly better agreement with the *monoclinic* model for all patterns below T_{Tb} (table 3), with the formal $C2'/m'$ magnetic space group. The refined lattice parameters clearly show (figure 6) that the degeneracy of the lattice parameters ($a = b$ *hexagonal* model, $a/\sqrt{3} = b$ *monoclinic* model) is lifted below T_{Tb} (i.e. $a/\sqrt{3} \neq b$, *monoclinic* model), due to the crystal symmetry decrease [4]. However, an attempt to use the orthorhombic and monoclinic models for the crystal structure (phase 1) in the analysis of the $x = 0.1$ and 0.25 sample data measured at MRPD did not improve the fit (table 3). This is probably due to the limited resolution of the MRPD.

The three models yielded very similar refined magnetic parameters (magnitude and orientation). The analysis yielded

Table 3. The reliability factors for the three crystallographic models used for LT diffraction.

		MRPD			HRPD		
x		$P6/mmm$	$Cmmm$	$C2/m$	$P6/mmm$	$Cmmm$	$C2/m$
0.05	χ^2	1.04	1.02	0.950	—	—	—
	R_{wp}	3.58	3.54	3.42	—	—	—
	R_{exp}	3.52	3.51	3.51	—	—	—
0.1	χ^2	0.662	0.722	0.677	0.563	1.02	0.408
	R_{wp}	5.13	5.36	5.19	12.1	16.3	10.3
	R_{exp}	6.31	6.31	6.30	16.12	16.12	16.11
0.25	χ^2	0.695	0.696	0.697	0.623	0.472	0.262
	R_{wp}	3.56	3.56	3.56	12.6	11.0	9.59
	R_{exp}	4.27	4.26	4.26	15.95	15.95	15.94

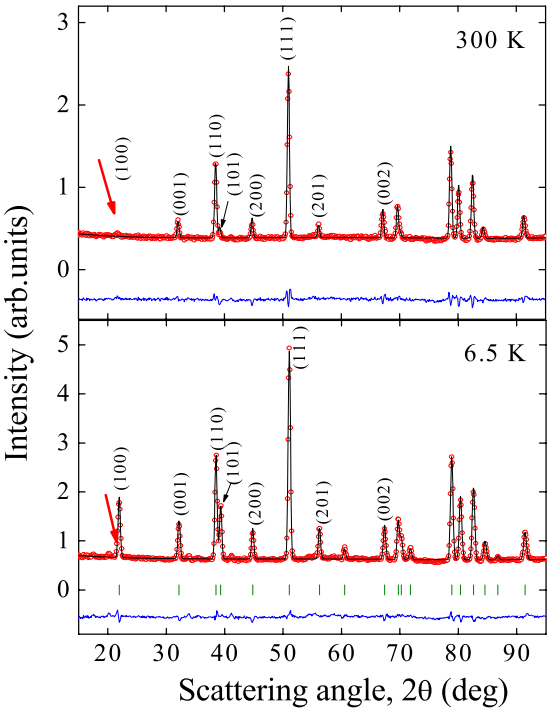

Figure 4. NPD of the $x = 0.05$ sample collected at MRPD at 300 K (top) and 6.5 K (bottom). Data (circles), Rietveld refinement profile (solid line) and their difference (solid line at the bottom) are depicted. Lines are indexed using the $P6/mmm$ lattice. The arrow points to reflection {100} (according to $P6/mmm$) which shows the most significant increase at LT.

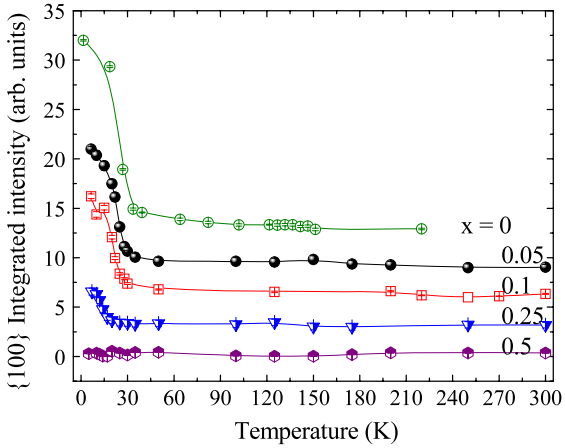

Figure 5. Integrated intensity of the {100} reflection (figure 4) as a function of temperature for $x = 0$ [3], 0.05, 0.1, 0.25 and 0.5 samples. The statistical error bars are smaller than the symbol's size. Constants: 12, 9, 6, 3, and 0 were added to the respective curves for clarity of presentation.

the temperature dependence of the magnitude of the ordered magnetic moment (figure 7), as well as the angle θ (not shown) in all samples which undergo a phase transition. The T_{Tb} linearly decreases as x increases, again in excellent agreement with AC and SQUID results (figure 3). Furthermore, the analysis yielded a clear decrease of the Tb magnetic moment from the free-ion value (table 2 and figure 7).

In order to study the expected symmetry reduction in the $x = 0.1$ and 0.25 samples, high resolution diffraction of both samples was collected at HRPD. At first, the LT HRPD data were analyzed following the same *hexagonal* model used for the analysis of the MRPD data. The refined crystallographic and magnetic values deduced from this analysis are in agreement with the values found in the MRPD analysis for both samples. However, refinements of the HRPD data yielded significantly better agreement (table 3) with the monoclinic model for all patterns below T_{Tb} (e.g. for the $x = 0.25$ sample at $T = 4.6$ K, R_{wp} is 12.6%, 11%, and 9.59% for *hexagonal*, *orthorhombic* and *monoclinic* models, respectively). The refined lattice parameters for both samples clearly show that the degeneracy (the equality of the normalized basal lattice parameters) of the lattice parameters a and b in the *hexagonal* model is lifted (i.e. $a/\sqrt{3} \neq b$) when analyzing the data using the *orthorhombic* or *monoclinic* models, in support of the expected orthorhombic/monoclinic distortion below T_{Tb}. Again, as is the case for the MRPD data, in the HRPD data analysis, no significant difference between the refined magnetic parameters (magnitude and orientation of magnetic axis) was detected when comparing the analysis of the *hexagonal* and *monoclinic* models. It is worth noting here that attempts to analyze the data for $T > T_{Tb}$ with the *monoclinic* model were made for all samples. These attempts yielded at every temperature either cell parameters with the ratio $a/b = \sqrt{3}$ (i.e. no orthorhombic/monoclinic distortion) or could not be converged.

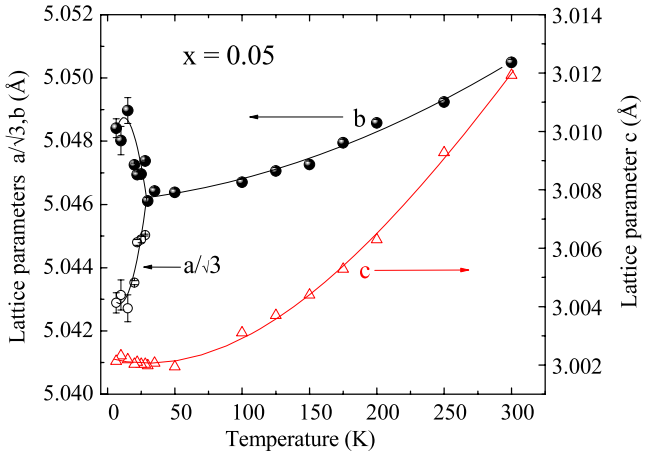

Figure 6. Lattice parameters of the $x = 0.05$ sample as a function of temperature. The *monoclinic* and *hexagonal* models were used for refinements below and above T_{Tb}, respectively. The lines serve as guides to the eye. Wherever not clearly indicated, error bars are smaller than the symbol's size.

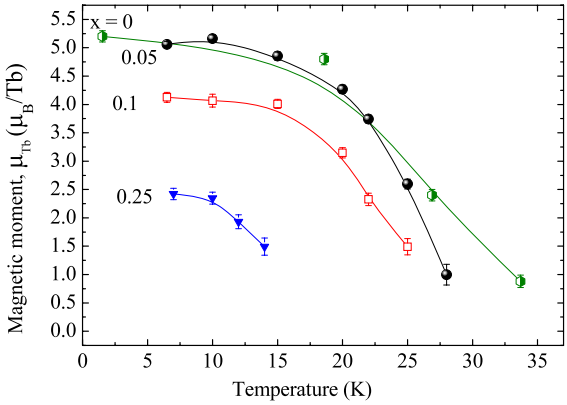

Figure 7. The ordered Tb magnetic moment versus temperature in the $x = 0$, 0.05, 0.1 and 0.25 samples. The data for $x = 0$ were taken from previous work [3].

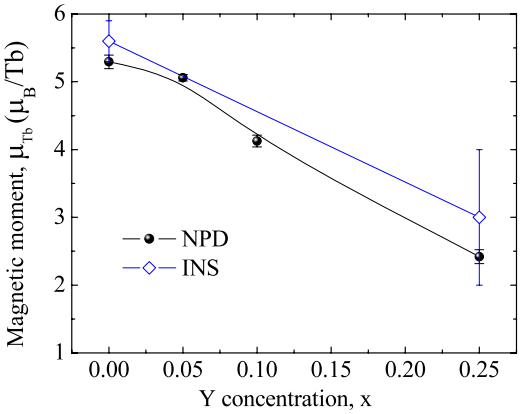

Figure 8. Tb ordered magnetic moment as a function of the Y concentration x, measured by NPD and INS.

As previously discussed [3], the magnetocrystalline anisotropy energy strongly depends on the magnitude of the magnetic moment ([3] and references therein). The Tb contribution to the magnetocrystalline anisotropy energy favors alignment of magnetic moments in the hexagonal basal plane ab, while the magnetocrystalline anisotropy energy contributed by the Co site favors alignment of magnetic moments along the hexagonal c axis. Dilution of the Tb site with the non-magnetic Y atom weakens the anisotropy contributed from the Tb site. Therefore, as x increases, it is expected to find the magnetic moments aligned closer to the hexagonal c axis. This is indeed the case (table 2(b)) for the $x = 0.05$ and 0.25 samples, for which $\theta = 76(2)°$, $50(6)°$ were observed. The anomaly at the $x = 0.1$ sample ($\theta = 46(3)°$) might be again related to the existence of impurities in this sample (see section 3). The refinements of the $x = 0.25$ sample were previously published [9, 11], yet the models were refined to the data again in this work using the most recent modifications applied. The results are in good agreement with what was previously published, although few differences exist, especially in the magnitude of the ordered Tb magnetic moments, due to some improvements made in the models during the work.

5. Discussion

In general, the magnetic properties of $Tb_{1-x}Y_xCo_3B_2$ presented here support our model of the magnetic behavior of the RCo_3B_2 compounds [3–5]. It is shown here that T_{Tb} depends on the dilution of the magnetic R site with a non-magnetic atom such as Y. T_{Tb} decreases from ~30 K for $x = 0$ [3] to ~14 K for $x = 0.25$ (figure 3). The absence of T_{Tb} in the $x = 0.5$ and 1 samples strongly supports our conjecture that the spin reorientation transition is driven by the R–R exchange interaction. Regarding T_{Co}, our AC susceptibility and SQUID magnetization results show that it does not change with the magnetic dilution of the R site. It also seems to be independent of R (i.e. $TbCo_3B_2$ [3], YCo_3B_2 [4] and $HoCo_3B_2$ [5]). These two properties (dilution and R independence of T_{Co}) show that T_{Co} is entirely governed by the Co–Co exchange interaction, regardless of the type of R atom.

NPD analyses show a considerable decrease in the magnitude of the ordered magnetic moment of the Tb ion, μ_{Tb}, with non-magnetic Y dilution (figures 7 and 8). In a recent study of the $x = 1$ and 0.25 samples using inelastic neutron scattering (INS) [11], it was shown that the ground state of the Tb^{3+} ion above T_{Tb} is a non-magnetic singlet. The magnetic ordering on the Tb sublattice was found to be 'self-induced'. This is a unique mechanism, where a fluctuating small magnetic exchange field causes admixture of the excited magnetic state into the non-magnetic singlet ground state (see [11] and references therein). This admixture leads to a small magnetic moment (in the ground state), resulting in an increase in the exchange field, which, in turn, will result in further increase in the magnetic moment. If the temperature is low enough, this process will continue until a critical point is reached, where magnetic order will set in. Such an admixed ground state can carry magnetic moments smaller than the fully quenched 6 μ_B. Diluting the Tb with non-magnetic

Y lowers the exchange interaction strength and leads to a further reduction in the Tb magnetic moment. In addition, the magnitudes of these ground state magnetic moments calculated from the INS measurements $\mu_{Tb} = 5.6(3)$ and $3(1)\ \mu_B$ for $x = 0$ and $x = 0.25$, respectively, are in good agreement with our NPD results (figure 8).

6. Conclusion

$Tb_{1-x}Y_xCo_3B_2$ solid solutions are paramagnetic at RT and undergo ordering of the Co sublattice at $T_{Co} \sim 150$ K for all x in $0 \leqslant x \leqslant 1$. This ordering temperature is independent of either x or R (lanthanide). At a lower temperature, T_{Tb}, an ordering of the Tb sublattice sets in for Y concentration of $x \leqslant 0.25$. For $x = 0.5$ no T_{Tb} was observed above 4 K. The value of T_{Tb} depends approximately linearly on the Y concentration. The magnetic ordering of the Tb sublattice drives the reorientation of the magnetic axis towards the basal plane (the Tb easy magnetic axis). This reorientation is accompanied by a symmetry decrease from hexagonal to monoclinic. Unexpectedly, it is found that the magnitude of the ordered magnetic moment of the Tb ion μ_{Tb} decreases with the Tb dilution. This observation was recently explained [11] by a unique mechanism of 'self-induced' magnetic ordering of the Tb sublattice.

Acknowledgment

The authors thank Israel Felner of the Hebrew University for his guidance with the SQUID measurements.

References

[1] Kuz'ma Y B and Bilonishko N S 1971 *Sov. Phys.—Crystallogr.* **18** 447
Kuz'ma Y B and Bilonishko N S 1974 *Kristallografiya* **16** 1030
[2] Hahn T (ed) 2005 *International Tables for Crystallography A* (Dordrecht: Kluwer, Academic)
[3] Dubman M, Caspi E N, Ettedgui H, Keller L, Melamud M and Shaked H 2005 *Phys. Rev.* B **72** 024446
[4] Sigalov O, Shames A I, Caspi E N, Dubman M, Ettedgui H, Goren S D and Shaked H 2005 *J. Appl. Phys.* **98** 074105
[5] Caspi E N, Dubman M, Ettedgui H, Shaked H, Short S and Jorgensen J D 2005 *Physica* B **359** 944
[6] Carvajal J R 1993 *Physica* B **192** 55
[7] Carvajal J R *An Introduction to the Program FullProf 2000*
[8] Niihara K and Yajima S 1973 *Bull. Chem. Soc. Japan* **46** 770
[9] Wolfson E J, Caspi E N, Avdeev M and Shaked H 2008 *J. Magn. Magn. Mater.* **320** L97
[10] Opechowski W and Guccione R 1965 *Magnetism* ed G T Rado and H Suhl (New York: Academic) p 105
[11] Rivin O, Osborn R, Kolesnikov A, Caspi E N and Shaked H 2008 *Phys. Rev.* B **78** 184424